remote sensing

MDPI

Article

Multidecade Trends of Sea Surface Temperature, Chlorophyll-a Concentration, and Ocean Eddies in the Gulf of Mexico

Geng Li [1], Zhankun Wang [2,3] and Binbin Wang [1,*]

[1] Department of Civil and Environmental Engineering, University of Missouri, Columbia, MO 65211, USA
[2] Northern Gulf Institute, Mississippi State University, Stennis Space Center, MS 39529, USA
[3] National Centers for Environmental Information (NCEI), NOAA, Stennis Space Center, MS 39529, USA
* Correspondence: wangbinb@missouri.edu

Abstract: This study characterizes the spatial patterns of the overall and monthly trends in sea surface temperature (SST) and chlorophyll-a (Chl-a) of the Gulf of Mexico (GoM) to investigate the seasonal variations in oceanic climate trends. We also investigate the trends in mesoscale eddies using three parameters to identify ocean-eddy-related energetic features in their area, strength, and intensity. Multidecadal remote-sensing-based observations of monthly SST, Chl-a, and sea surface height are used to detect trends at both basin and grid scales. Prominent warming trends are found in most regions of the GoM in all months, with the largest trends in the northern GoM. Winter cooling trends are also detected along the Texas and Florida coast. The overall summer warming trend (~0.22 °C/decade) is larger than the winter trend (~0.05 °C/decade), suggesting seasonal variations of increase in SST with warming. Chl-a trends and variations are confined on the continental shelf and slope in the northern GoM. The largest increase trends are found near the Mississippi River Delta. No obvious Chl-a trend is detected in the deepwater of the GoM, consistent with previous studies. Small but significant changes are found in eddy characteristics, indicating the eddy activities might be slowly affected by climate change in the GoM. The detailed monthly trends at per-grid scale are valuable for regional resource management, environmental protection, and policy making in the GoM.

Keywords: Gulf of Mexico; sea surface temperature; chlorophyll-a; ocean eddies; trends

check for updates

Citation: Li, G.; Wang, Z.; Wang, B. Multidecade Trends of Sea Surface Temperature, Chlorophyll-a Concentration, and Ocean Eddies in the Gulf of Mexico. *Remote Sens.* **2022**, *14*, 3754. https://doi.org/10.3390/rs14153754

Academic Editors: Dionysios E. Raitsos and Nicola Montaldo

Received: 7 June 2022
Accepted: 1 August 2022
Published: 5 August 2022

Publisher's Note: MDPI stays neutral with regard to jurisdictional claims in published maps and institutional affiliations.

Copyright: © 2022 by the authors. Licensee MDPI, Basel, Switzerland. This article is an open access article distributed under the terms and conditions of the Creative Commons Attribution (CC BY) license (https://creativecommons.org/licenses/by/4.0/).

1. Introduction

The Gulf of Mexico (GoM) is one of the most economically and ecologically important marginal seas in the world ocean. The GoM plays an important role in the transport of heat, nutrients, biomass, and salt from the Caribbean Sea to the North Atlantic Ocean via the loop current [1]. The ocean dynamics, heat storage, primary production, and habitat of marine organisms, fish, and marine mammals in the GoM are critical to the weather and climate, economy, and recreation of Central America, the United States, and the Caribbean Sea. The GoM is a main habitat for many marine mammals, sea turtles, coastal and pelagic fish, birds, and other species [2]. It is also the primary offshore source of oil and gas in the U.S. Hence, understanding the spatial and temporal patterns of changes in the GoM surface ocean and how they evolve over time are important to many aspects in marine resource managements, sustainable development and conservation, extreme weather forecast, and socio-environmental management. For example, sea surface warming has a large contribution to the recent increase in Atlantic hurricane activity [3].

Oceanic environmental changes have been a general interest and hot topic for both the world ocean and regional seas, such as the GoM. Regional climate change is especially important to local environment protection and resource management. Dunstan et al. [4] have studied the global patterns of change and variation in sea surface temperature (SST) and chlorophyll-a concentration (Chl-a) and found both positive and negative correlations

between them with great spatial variations. They suggest that over decadal time scales, both trend and variation in SST, Chl-a, and their covariance are highly spatially heterogeneous and, therefore, monitoring and resource management must be regionally appropriate. However, previous research on the warming trend and Chl-a change in the GoM is limited. Because of the heterogeneity of climate and its change, we investigate the regional trends and their monthly variations in SST and Chl-a in the GoM.

Muhling et al. [5] have discovered that the temperature has risen approximately at a rate of 0.22 °C decade^{-1} in the northern GoM between 1985 and 2008. Moreover, they found a close relationship between the increase in pelagic fish larvae and warmer years. Glenn et al. [6] have examined the SST warming in the Caribbean and the surrounding region and found that the greatest warming is in the northern GoM and south America. Muller-Karger et al. [7] have studied the patterns of seasonal variations and trends of SST, wind speed, sea surface height anomaly (SSHA), Chl-a, and net primary production (NPP) in surface water of the central GoM (water depth > 1000 m) between the early 1980s and 2012. During their study period, SST, wind, and SSHA measured a persistent increase, while Chl-a and NPP did not show significant trends. Monthly average SST in the GoM shows a clear annual cycle with the highest SST of 29–30 °C measured between July and September and the lowest SST found in February and March [8]. On average, the warming trends in the deepwater of the GoM range from 0.17 to 0.3 °C per decade [7]. Changes in SST are often associated with changes in other variables, such as Chl-a and primary productivity [9]. The seasonal variation of phytoplankton concentrations in GoM is more constrained on the continental shelf, with the highest values (>0.2 mg/m^3) in December to February and the lowest values in May–July (<0.06 mg/m^3) [8]. Muller-Karger et al. [7] have shown that trends of some variables have seasonal variations by comparing the trends between summer and winter. For example, there is no significant trend in wind intensity in summer months (July–September), but an increase trend in winter (November–January) when seasonal winds are highest. No obvious difference is found between summer and winter warming trends and no significant decadal scale trend in Chl-a concentration is detected in the deepwater of the GoM [7]. Below the surface, the GoM also experienced apparent warming in recent decades based on the temperature profiles [10] and moored observations [11].

Ocean circulation of the surface water in the GoM is dominated by the loop current (LC) and associated mesoscale eddies [12,13]. The LC enters the GoM via the Yucatan Channel and brings warm and saline Caribbean water into the gulf. It stretches northward and can reach as far north as 29°N, around the Mississippi River delta. Anticyclonic loop current eddies (LCE) are detached from the LC on time scales of approximately 3–17 months [14–16]. After detached, an LCE drifts westward and decays in the western GoM. Moreover, smaller cyclonic eddies (known as the LC frontal eddies, LCFE) also formed around the northern tip of an extended LC [17], which greatly affects the LCE formation and detachment [18,19]. LC patterns and eddy characteristics in the GoM have been extensively studied using satellite SSH fields [20,21], in situ observations from drifters, and hydrographic surveys [22–24] and models [16,25]. Both LCE and LCFE play an important role in the redistribution of physical and biochemical properties in the GoM [26]. LCE can stimulate productivity in the GoM in the winter via mixed layer deepening, which brings nutrient-richer water into the mixed layer [27]. The LC, LCE, and LCFE influence processes on the continental shelf and slope in the northern GoM in all seasons [28] and generate cross-isobath transports to advect the Mississippi and Atchafalaya Rivers' water and materials offshore [29–31].

In previous trend studies in the GoM, seasonal variations are typically removed by subtracting the long-term monthly climatology from the monthly field for that variable [7]. In this manuscript, one of the focuses is on the seasonal variations of the long-term trends by examining the monthly trends at each grid. This allows us to investigate if seasonal variations of long-term trends in SST and Chl-a can be detected. Multiple decades of daily satellite observations of SST and Chl-a are used. SST shows the thermodynamics of the

sea surface water, while Chl-a is an index of the biomass of phytoplankton of the surface ocean. We also investigated the trends in mesoscale eddies using three parameters to identify ocean eddies and quantify their sizes, total strength, and intensity. The purpose of this study is to expand the knowledge of the long-term trends of key environmental change parameters (temperature, Chl-a, and eddy activities) in the GOM using satellite observations. This study is particularly aimed for investigating the seasonal variations and phase shift of the long-term change in temperature and Chl-a, which is lacking in the literature. We also investigated changes in eddy properties to examine if the recent warming has any long-term impact on the eddy characteristics.

2. Materials and Methods

2.1. Study Area

The Gulf of Mexico is a semi-enclosure basin, bounded on the north by the United States of America (USA), on the southwest and south by Mexico, and on the southeast by Cuba (Figure 1). It connects the Caribbean Sea and northern Atlantic Ocean via two narrow channels, the Yucatan Channel between Mexico and Cuba and the Straits of Florida between Florida, USA and Cuba (Figure 1). The GoM has broad continental shelfs at most points along the coast with half of the basin consisting of shallow continental-shelf water (see topography map in Figure 1).

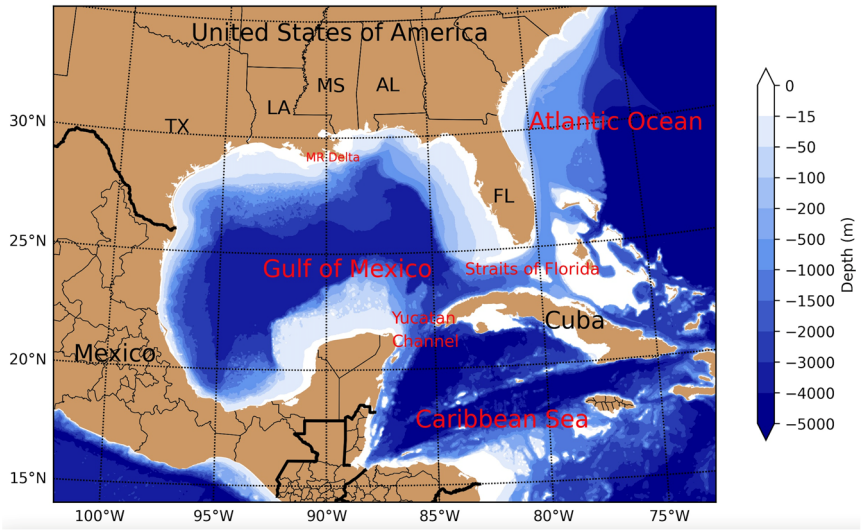

Figure 1. Map of the Gulf of Mexico and its surrounding oceans with colormap of seafloor topography to show the geographic features of the study region. The vertical scale is water depth (m). TX: Texas; LA: Louisiana; MS: Mississippi; AL: Alabama, FL: Florida; MR Delta: Mississippi River Delta.

2.2. Data

The data of SST is obtained from the optimum interpolation result of Advanced Very High Resolution Radiometer (AVHRR) infrared satellite SST data and Advanced Microwave Scanning Radiometer (AMSR) on the NASA Earth Observing System satellite SST data. The SST data have a 0.25° spatial resolution and 1 day temporal resolution. The data period used in this study is 1982–2019. The data is available through https://psl.noaa.gov/data (accessed in January 2020).

The data of Chl-a concentration (mg/m^3) are obtained from the European Space Agency (ESA) Ocean-Colour Climate Change Initiative (OC-CCI) project [32]. The data is the merged remote sensing reflectance from various satellites missions (i.e., SeaWiFS, MERIS, and Aqua-MODIS). The Chl-a data has a 4 km spatial resolution and 1 day temporal resolution. The data period used in this study is 1997–2018. The data is available through https://resources.marine.copernicus.eu/products (accessed in January 2020).

The data of SSH is obtained from the Archiving, Validation and Interpretation of Satellite Oceanographic (AVISO) data set, which is distributed by the French National Centre for Space Studies (CNES). The data is a multimission altimeter product which contains Sea Level Anomaly Height (SLA-H), Absolute Dynamic Topography Height (ADT-H), and Geostrophic Velocities (SLA-UV and ADT-UV) at 0.25 degree and daily resolution. The data period used in this study is 1993–2019. The data is available through https://www.aviso.altimetry.fr/en/home.html (accessed in January 2020).

2.3. Method

2.3.1. Linear Regression and Monthly Downsample Analysis

Linear regression is the basic method we used to determine the overall trend of data over the period of interests in our study. All time series data of SST, Chl-a, and ocean eddies are processed using linear regression to evaluate their temporal changes. For instance, linear regression is applied to the daily value of spatially averaged temperature in the entire GoM to determine the temperature trend in the GoM (i.e., the slope of linear regression result). Linear regression is also carried out on the per-grid scale to evaluate the grid-specific trend of each variable. This allows us to examine the spatial variation of the trends, which is important to the resource management.

To obtain better understanding of how ocean dynamics evolved in specific calendar months over the last several decades, we chose to downsample the data (i.e., SST and Chl-a) by each month so that their long-term trend in each month can be calculated. Linear regression is used to determine the month-specific trend using the monthly downsampled data, i.e., the daily data in each specific month. We calculated month-specific trends for SST and Chl-a for the entire GoM as well as spatial distribution of month-specific trends in each available grid point in the GoM. Two cut-off thresholds were chosen to help understand the trend of each variable. For the time series of a spatially averaged variable (e.g., time series of GoM temperature), p-value < 0.05 was selected as the criterion of the significant test. For grid specific data, p-value < 0.1 was used as the criterion of the significant test to relax the sensitivity of the high spatial resolution data.

2.3.2. Phenology Analysis

Trigonometric function can be used to describe the phenological information of the SST data. Following Lian [33], the SST data can be decomposed using:

$$\mathrm{SST} = \underbrace{kt}_{\text{trend}} + \underbrace{A\sin\left(\frac{2\pi}{T}(t+\psi)\right)}_{\text{phenological term}} + \underbrace{B}_{\text{base term}} \quad (1)$$

In Equation (1), A, T, and ψ are amplitude, period, and phase (unit: day) of the phenological change in the SST, respectively. This equation defines how temperature would vary in the phonologic cycle with a period of one year, i.e., T = 365 days. When phase $\psi = 0$, the peak of sinusoidal function occurs at $2\pi t/T = \pi/2$, i.e., t = 91.25 yearday. Likewise, the trough occurs at $2\pi t/T = 3\pi/2$, i.e., t = 273.75 yearday. The physics meaning of phase value indicates shift of cycle earlier by the correspondent days (i.e., $-\psi$ days) or shift later by days of $365 - \psi$. For instance, ψ = 240 means that the peak temperature would occur on the yearday of 91.25 + (365 − 240) = 216.25, and the trough of temperature would occur on the yearday of 273.75 − 240 = 33.75.

In this study, the trend of SST data is removed so that the phenological equation can be fitted to the data using Equation (1) using a nonlinear least-square approach to obtain a phase value. Similarly, the phase of Chl-a is calculated using the same approach. Figure 2 show an example of phenological analysis for SST and Chl-a at selected locations in the GoM. A clear seasonality can be observed in both SST and Chl-a data, where the phase information can be obtained using the phenology analysis.

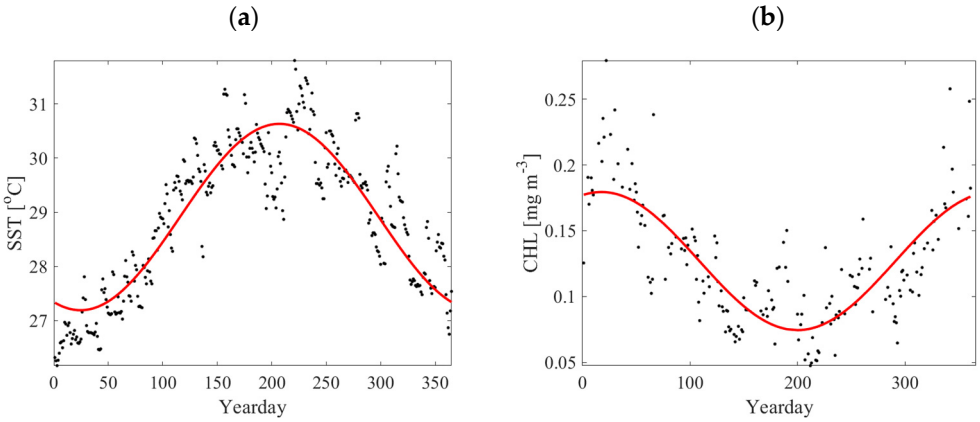

Figure 2. An example of phenological analysis for (**a**) sea surface temperature (SST); (**b**) chlorophyll-a concentration (Chl-a). The phase values in these two regression lines are yearday of 249.25 and 73.82, respectively. (Note that the phase yeardays do not correspond to peaks or troughs in the curve. See explanation of the phase in Equation (1)).

2.3.3. Energetic Features of Ocean Eddies

SSH data are used to calculate geostrophic velocity:

$$u = -\frac{g}{f}\frac{\partial \eta(x,y,t)}{\partial y} \tag{2}$$

$$v = \frac{g}{f}\frac{\partial \eta(x,y,t)}{\partial x} \tag{3}$$

where u and v are the east and north components of geostrophic ocean surface velocity, $\eta(x,y,t)$ is the spatially and temporally varying SSH, g is gravitational acceleration, and f is Coriolis parameter which is a function of latitude [34,35]. The following three eddy relevant parameters are calculated:

(1) Vorticity:

$$\omega_z = \frac{\partial v}{\partial x} - \frac{\partial u}{\partial y} \tag{4}$$

(2) Swirling strength [36]:

Two-dimensional velocity tensor defined by the geostrophic velocity gradient is [37]:

$$D = \begin{bmatrix} \frac{\partial u}{\partial x} & \frac{\partial u}{\partial y} \\ \frac{\partial v}{\partial x} & \frac{\partial v}{\partial y} \end{bmatrix} \tag{5}$$

The velocity gradient tensor either has two real eigenvalues or a pair of complex conjugate eigenvalues $\lambda_{cr} \pm i\lambda_{ci}$. λ_{ci} can be used to quantify the strength of the vortex swirling motions.

(3) Okubo–Weiss parameter [38]:

$$W = S_n^2 + S_s^2 - \omega_z^2 \tag{6}$$

where S_n and S_s are normal and shear strain, respectively.

In this study, we use the above three parameters to represent the energetic features of ocean eddies and quantify their sizes, strengths, and intensities. Our calculation does not identify the actual ocean eddies, rather, it provides important characteristics associated with the ocean eddies (e.g., strain, swirling). For instance, both cyclonic and anticyclonic eddies in the GOM are surface intensified in terms of vorticity and swirling strength [13], and therefore can be easily detected from SSH imageries. The absolute value of vorticity

and Okubo–Weiss parameter are used to describe the strength, regardless of the direction of rotation. They are denoted as absolute vorticity and absolute Okubo–Weiss parameter in this study. Specifically, we define a threshold for each parameter at 90% of cumulative distribution of the time-averaged value at each grid in the GoM. This threshold identifies the strongest eddy-like features as a function of time and space. The area, strength, and intensity of these energetic features are calculated after thresholding. Figure 3 shows an example of the identified most energetic features of eddies in absolute vorticity, swirling strength, and Okubo–Weiss parameter on 21 July 2018. The relation and difference in eddy detections using these parameters are beyond the scope of this study. Nevertheless, all parameters can be used to represent the dynamics of eddies in the GoM. The total strength is defined for each parameter as the summation of the parameter for all identified areas (e.g., total strength defined using swirling strength is the sum of the swirling strength of all eddies). The intensity is defined as the total strength divided by the total area occupied by these features, i.e., strength per unit area. Linear regression is used to determine whether there are changes in each parameter of the ocean eddies in the GoM.

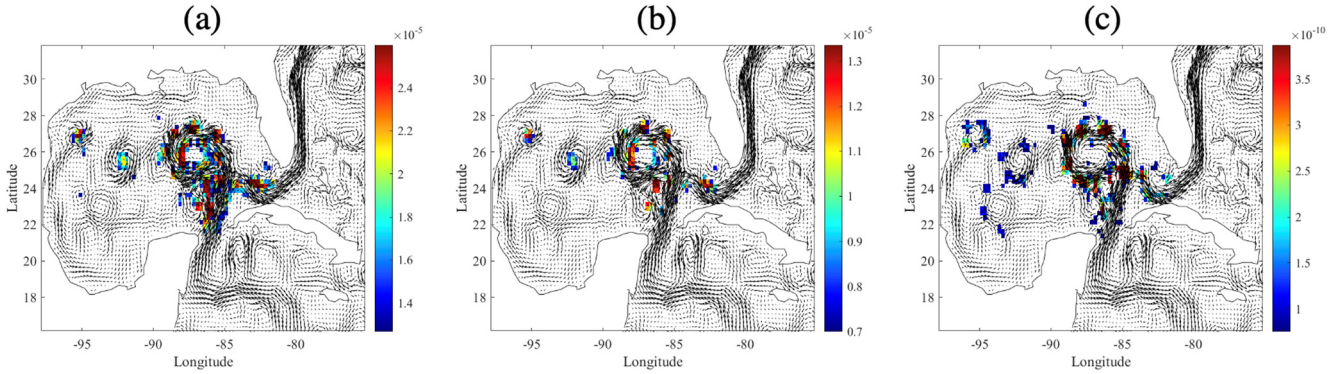

Figure 3. An example of eddy identification on 21 July 2018 using three parameters: (**a**) absolute vorticity, unit: s^{-1}; (**b**) swirling strength, unit: none; (**c**) Okubo-Weiss parameter, unit: s^{-2}. The areas with 90 percentile of each parameter are shown. Velocity vectors are plotted for reference.

2.3.4. Source of Error

We note that grid data of sea surface parameters used in this study are the processed data, which are produced using original satellite observations with necessary interpolation and adjustments. Hence, different algorithms could be a source of uncertainty and error in our analysis. However, we note that our analysis is based on the daily time-series data over a few decades. The error due to the data interpolation should be relatively small.

3. Results and Discussion

3.1. Sea Surface Temperature

3.1.1. Overall Linear Trend

Figure 4a shows the monthly SST variation during the 1982–2019 period and the linear regression result superimposed on the monthly plot. The best-fit slope (warming trend) is found to be 0.158 °C/decade, giving an overall 0.6 °C increase in SST across the entire GoM during this period. This warming trend is comparable to the value estimated by Glenn et al. [6] but slightly smaller than the estimates in Muller-Karger et al. [7] and Muhling et al. [5]. The time series of the monthly temperature shows the annual SST cycle with minima (22–24 °C) around February and maxima (28–30 °C) in August. The anomalously cold winters of 2010 and 2011 (see also Muller-Karger et al. [7]) are also shown in Figure 4a. Figure 4b shows the map of temperature change per decade using linear regression at each available spatial location. Figure 4c plots the mean SST in the GoM. The mean SST shows a clear spatial gradient relevant to the latitude, i.e., lower SST in higher latitude regions (Figure 4c) except for the LC region. Within the gulf, the increase in SST also shows a spatial gradient relevant to latitude but in an opposite direction as that in

the mean SST (Figure 4b), i.e., higher SST rise in higher latitude regions. This implies that the northern continental shelf and slope in the GoM are likely more affected by oceanic surface warming. The general SST rise is about 0.1–0.2 °C/decade in the gulf, and higher temperature rise is observed in the coastal region of the northern gulf. The highest value is close to 0.5 °C/decade in the Mississippi delta region.

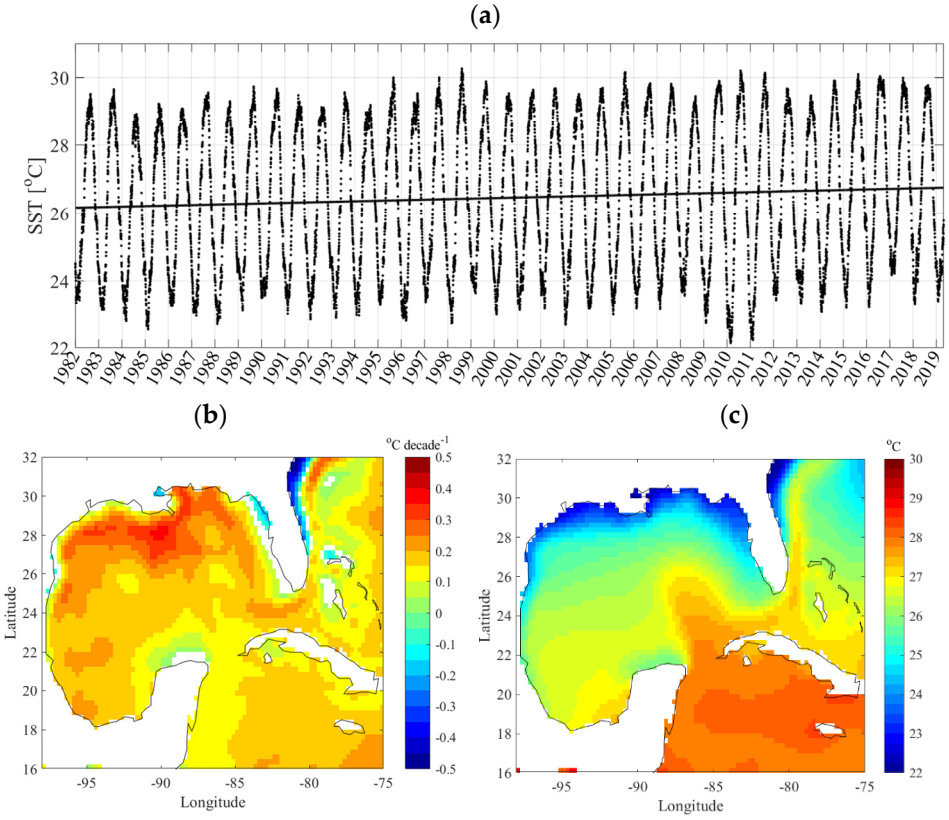

Figure 4. (**a**) Linear regression of sea surface temperature (SST) for the entire Gulf of Mexico (GoM) during the 1982–2019 period. The slope of linear regression indicates the increase in SST at a rate of 0.158 °C/decade; (**b**) spatial distribution of linear trend (°C/decade) of the SST in the GoM during the 1982–2019 period. Regressions with *p*-value > 0.1 are excluded in the plot; (**c**) spatial distribution of mean SST in the GoM during the 1982–2019 period.

3.1.2. Month-Specific Trend

An example of month-specific SST regression is given in Figure 5a using the largest (October) and smallest (January) rate of change. The data shows October has a relatively larger rate of increase in SST than January during the 1982–2019 period. The month-specific regression shows that the trend of SST change differs in different months in the GoM (Figure 5b). The data show that the rate of SST increase is weaker during winter (December to February) in the GoM. The different warming rates between winter and summer (Figure 5) suggests that the amplitude of the annual SST cycle increases with oceanic warming. Not only does the water become warmer and warmer, the seasonal variations of SST also become larger and larger, which might cause more extreme events (e.g., marine heat waves) in the GoM [39–41].

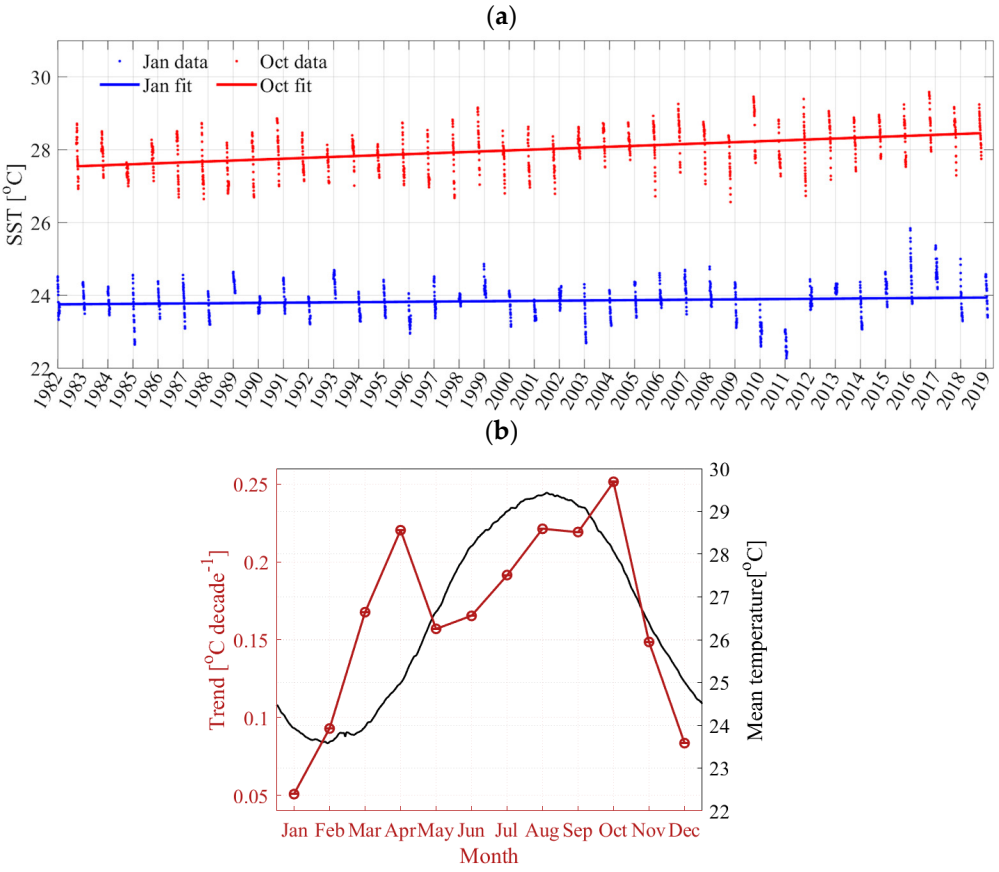

Figure 5. (**a**) An example of linear regression of the SST using monthly downsampled SST data (spatially averaged daily SST in the Gulf of Mexico for January and October, respectively). The rate of increase is 0.051 and 0.252 °C/decade for Janurary and October, respectively. (**b**) Rate of increase (trend) in SST for each month in the GoM (red line). Plot of the trend is superimposed onto the monthly mean SST data (black line).

Figure 6 shows the spatial distribution of the linear trend of SST change in each month from the monthly subsampled data. Strong spatial and seasonal variabilities are observed from these plots. During the wintertime, the coastal region of Texas and Florida shows a decreasing trend of SST (see December–February), whereas the Mississippi/Alabama coast remains a warming trend throughout the year. The coastal cooling trend could cause more coastal cold spells during wintertime in the northern GoM, which is another type of extreme event responsible for the coastal fish killing in the northern GoM [42]. The northern gulf shows a stronger warming trend compared with the rest of gulf region in the wintertime. This is a localized feature that is associated with temporal variability of the SST, which might be the result of strengthened westward wind in the winter (increase at >0.36 m/s per decade [7]). Chang and Oey [43] have found that wind-induced currents along the northern shelf of the GoM play a critical role in the westward heat redistribution. Westward wind is strongest in winter and weak in summer [43], and the wind magnitude increase is also larger in winter [7]. It will be interesting to examine the increased westward heat transfer due to the strengthened westward wind in the future. In spring and fall seasons, the general location of LC shows a weaker warming trend than the rest of the gulf. This could be due to the SST remaining at a relative stable condition in the loop current, which is weaker during these seasons [44,45]. Many studies of the LC in the GoM suggest that the northward maximum penetrations of LC occur on average in winter and summer [44–46], and more eddies tend to be shed in winter and summer as well [16]. During the summertime, the entire gulf has a uniformly increasing SST and no obvious spatial pattern is observed, as found in Liu, et al. [47]. The strongest warming trends occur in April and October,

dominating the warming trend of the entire GoM. The seasonal variations of the per-grid trends in Figure 6 have overall similarities as the trends in Glenn et al. [6], but our monthly per-grid trends reveal more details.

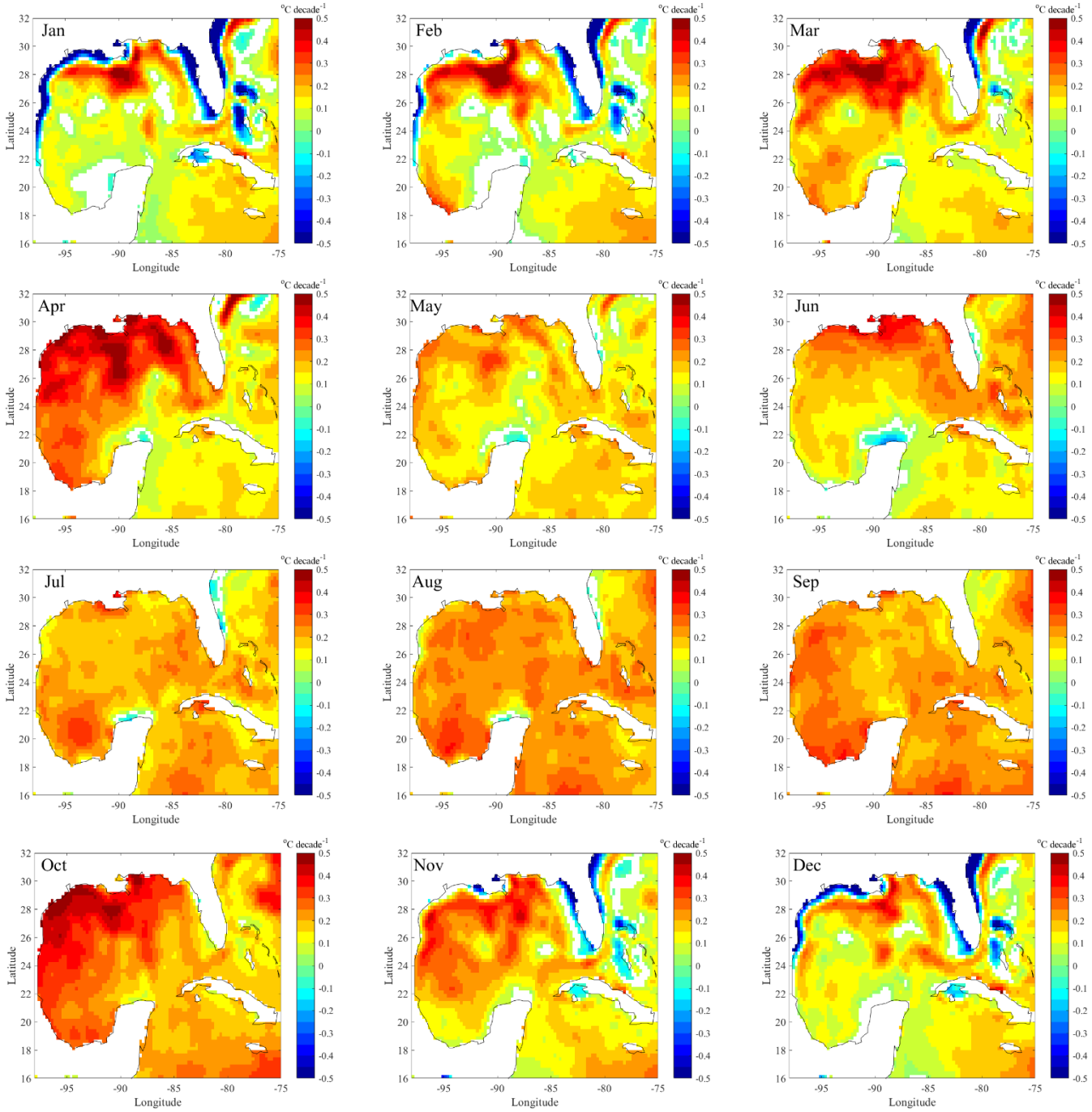

Figure 6. Spatial distribution of the month-specific SST trend (°C/decade) during the 1982–2019 period. Regressions with p-value > 0.1 are excluded in the plot. All color bars show −0.5 to 0.5 °C/decade for the rate of change in SST.

We note that p-value < 0.1 can only be considered as weakly evidenced trends. The threshold of 0.1 is chosen because of the existence of high variability associated with ocean eddies. It is important to mention that insignificance of the trend (p-value > 0.1 in the regression) indicates strong variations in the region. The insignificance does not necessarily mean that these regions experience different long-term trends from other regions where

significant trends are found. For instance, the coastal region of the West Florida Shelf has been reported to be a highly dynamical region of LC system [48].

3.1.3. Phonology Changes

Figure 7 shows the spatial distribution of the SST phase (Figure 7a) and the change in phase in the GoM (Figure 7b). The data show that the overall SST phases in the GoM is within 210~255 days, where the northern coast of the GoM has the largest phase values. Through regression, we find an increase in the phase value (1~4 days) in the northern coast of GoM, whereas the rest of the GoM does not show statistical trend of phase shift (shown in blank). A small region of phase shift at the north of the Yucatan is where cyclonic eddies are known to frequently sit (e.g., Nickerson, et al. [49] and Yang, et al. [50]). The phase shift in this region may indicate a potential change in cyclonic eddies. The phase increase in the coastal region shows that the phenological cycle of SST shifts towards earlier time, i.e., earlier summer (winter). This also suggests the coastal regions are more easily affected by the climate change than the deepwater.

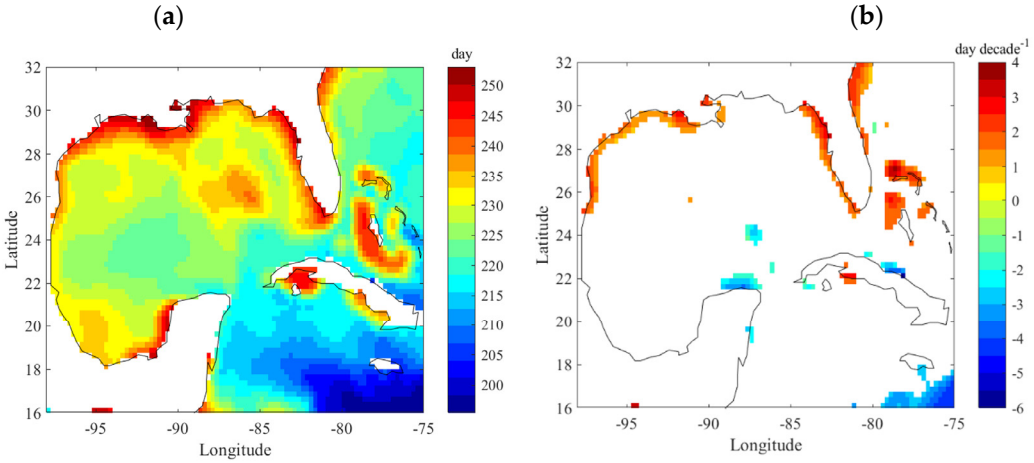

Figure 7. (**a**) Mean phase of SST during the 1982–2019 period; (**b**) change in phase for SST during the 1982–2019 period, where the results with p-value > 0.1 are excluded in the plot.

3.2. Chlorophyll-a

3.2.1. Mean Concentration and Trend

The mean Chl-a concentration and its rate of change in the GoM during the 1997–2018 period are shown in Figure 8. Substantially larger concentrations are present in the coastal region with favorable nutrient levels (Figure 8a). In addition, a quite strong increase in Chl-a concentration is found around the Mississippi River Delta (MRD). The causes of the Chl-a concentration increase around the MRD are unclear. The phytoplankton growth is more nutrient-limited in the GoM [7]. Excess nutrients transported by the Mississippi River are one of the major factors controlling the Chl-a concentration on the continental shelf of the northern GoM, including the Mississippi Delta. Stackpoole et al. [51] have conducted a comprehensive study on the annual river nutrient loads and trends near the outlet of the Mississippi River between 1975 and 2017. During the period of our Chl-a observations, the total nitrogen and nitrite plus nitrate likely had a slightly increase trend, while ammonia had a clear declining trend. The total phosphorus had an increasing trend, but orthophosphate had a decreasing trend [51]. More investigations are needed to determine which nutrition constituent(s) might be responsible for the enhanced MRD Chl-a concentration observed in Figure 8. Furthermore, any change in wind-induced Ekman suction, convective mixing caused by cold weather events, coastal circulations, and mesoscale eddy activities could all contribute to the Chl-a concentration change, which makes it even harder to determine the controlling factors of the Chl-a trend. In the Florida coast, a decrease in Chl-a concentration is found. In offshore regions of the gulf, the change in Chl-a concentration is limited in comparison with the coastal areas, which is consistent

with the findings in Muller-Karger et al. [7] that no obvious Chl-a trend could be detected in the deepwater (depth > 1000 m) of the GoM.

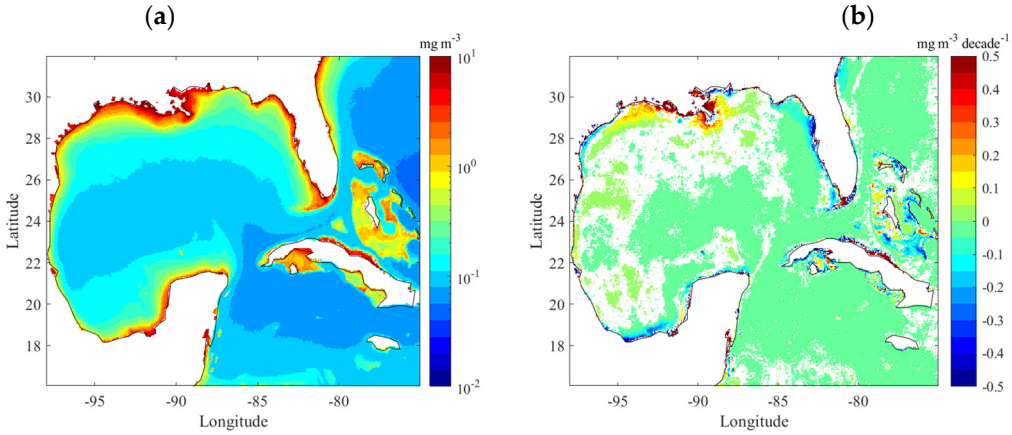

Figure 8. (**a**) Spatial distribution of mean Chl-a concentration in the GoM. Data is from 21 September 1997 to 31 December 2018. (**b**) Spatial distribution of rate of change in Chl-a concentration using linear regression. Data is not shown for p-value > 0.1.

Mean Chl-a concentration and its rate of change during each month is plotted in Figure 9. Chl-a concentration is found peaking during wintertime (0.6–0.9 mg/m^3) and remaining relatively low in value (0.4–0.5 mg/m^3) from late February to early June and August. The magnitude of the winter Chl-a peak is closely related to the intense mixing of the water column in the winter, which is further controlled by stratification (temperature) and wind [7,52]. In cooler and windy winters, convective mixing and Ekman suction bring more nutrients from the deepwater into the mixed layer, which can result in the "spring" blooms and higher Chl-a concentration at the surface in winter. In contrast, milder wind and warmer temperature lead to lower than normal Chl-a concentration in the winter [7]. Pasqueron de Fommervault et al. [53] have confirmed that the deepening of the mixed layer is the dominant factor causing the GoM Chl-a surface increase in winter based on subsurface profile data from biogeochemical Argo profiles. However, rather than a net biomass increase, they suggest that the surface increase in Chl-a concentration is more due to a vertical redistribution of subsurface Chl-a, instead of due to nutrient-induced new production. Nonetheless, the surface Chl-a in the winter is controlled by both surface and subsurface processes and should be investigated more in the future. There is a slight increase in Chl-a in late June and early July, which is likely associated with the offshore dispersal of the Mississippi River and other coastal waters [7,8,54] due to the prevailing southwesterly winds during this period [55]. A large change in Chl-a in January is found, i.e., about 10% changing rate per decade in comparison with the mean value of Chl-a concentration. The data also show a noticeable negative rate of change in May–July.

Figure 10 shows the month-specific trend of Chl-a concentration change in the GoM. Rich and dynamic patterns are found from monthly data, showing quite strong trends of changing primary production at various regions in the gulf that are relevant to calendar months. Obvious trends are constrained in coastal regions. In general, Chl-a concentration has an increasing trend close to the Mississippi River Delta region and Texas–Louisiana–Alabama coast. However, quite strong decreasing trends are present in the west of the Mississippi River Delta in February and March. Decreasing trends are often found at the Florida coast and the southwest gulf in the coastal region of Mexico. A more offshore Chl-a increase area is observed in July and August south of the Mississippi Delta. Muller-Karger et al. [7] have also found high levels of Chl-a and NPP occur regularly in July and August at the same region. They conclude that the high Chl-a and NPP are related to the east and southward dispersal of Mississippi water. We suspect that the Chl-a increase off the Mississippi Delta is also related to the dispersal of Mississippi water.

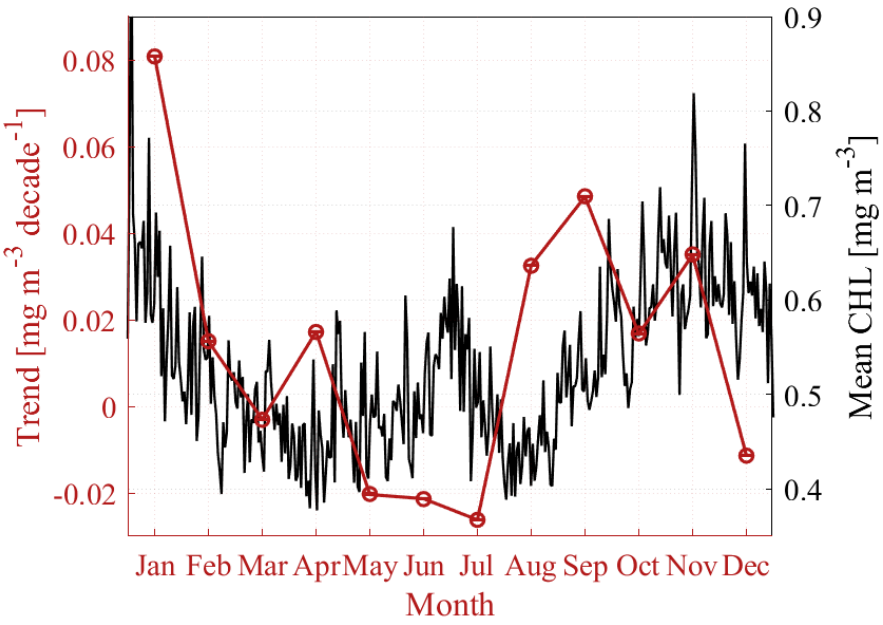

Figure 9. Mean Chl-a concentration (black line) in the GoM and the linear trend of Chl-a change (red circle and line) during the 1997–2018 period.

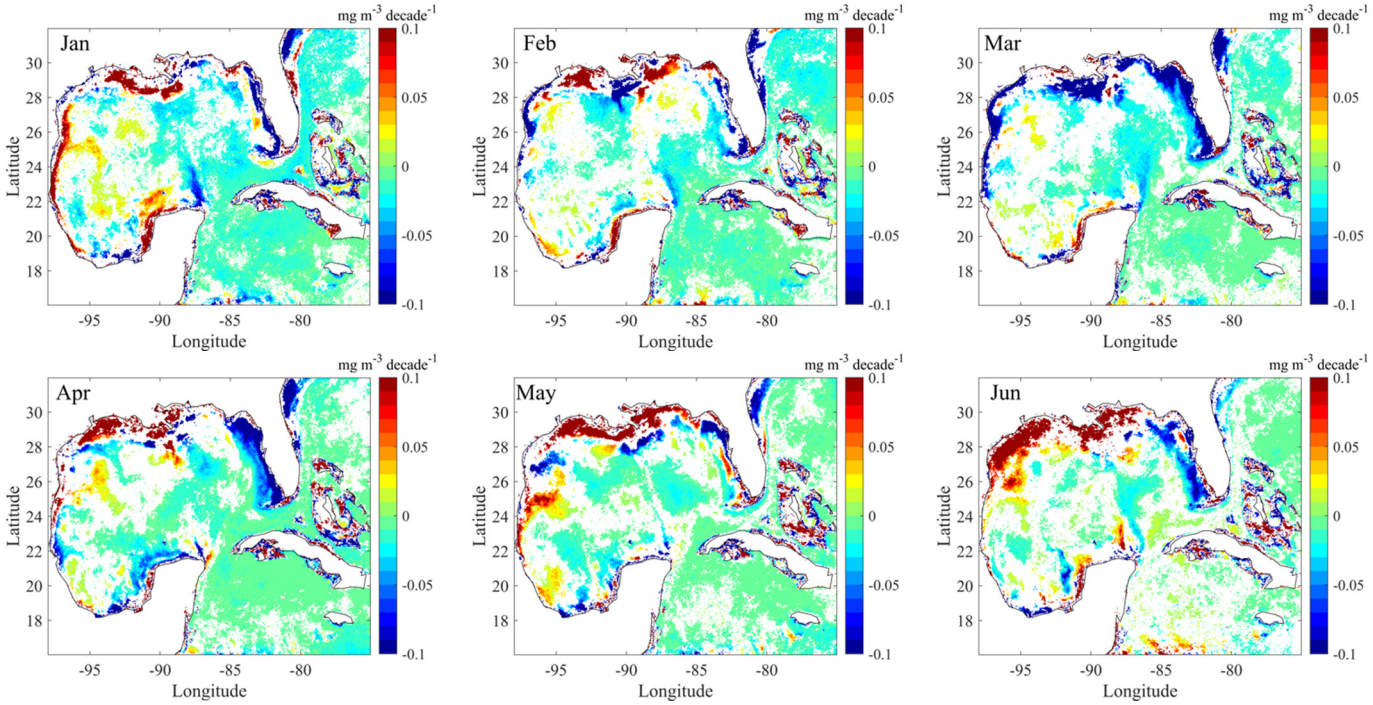

Figure 10. *Cont.*

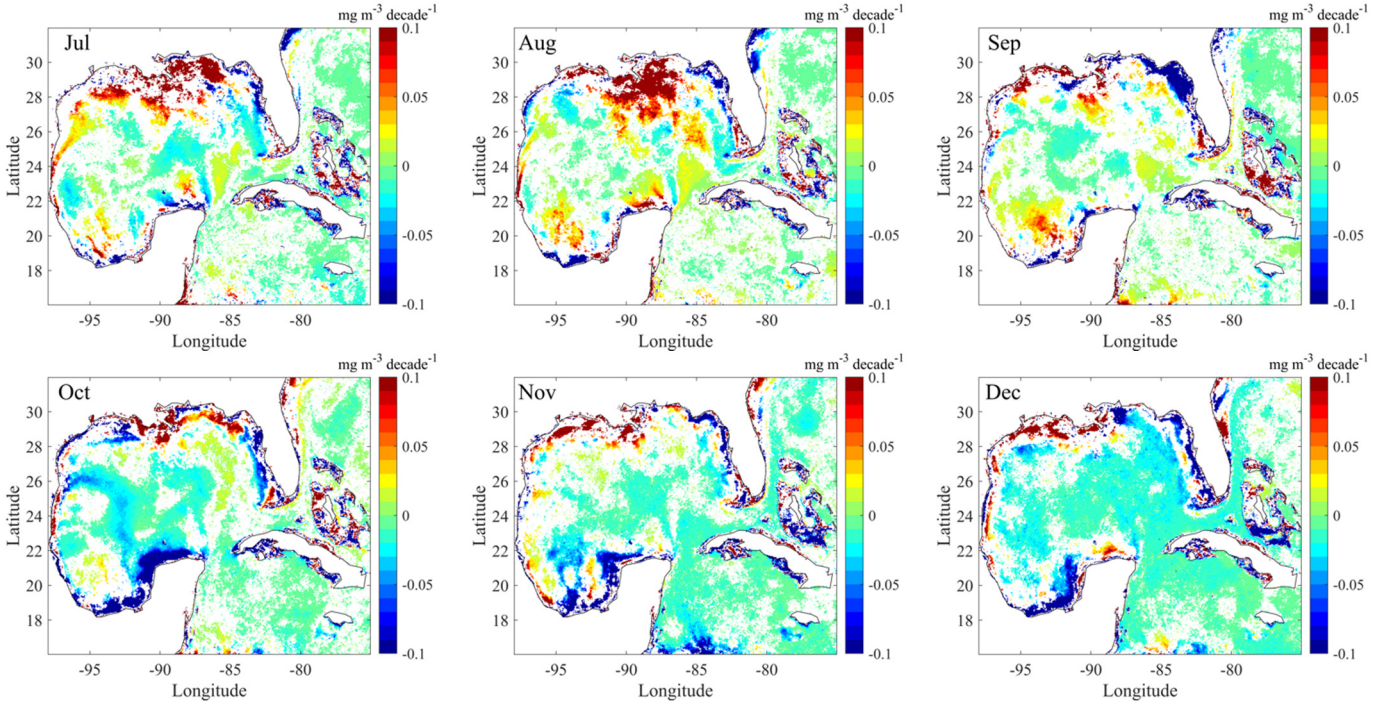

Figure 10. Spatial distribution of the month-specific trend of Chl-a concentration in the GoM.

3.2.2. Phase and Phase Shift

Figure 11 shows the spatial distribution of the mean phase of Chl-a concentration and the phase shift during the 1997–2018 period from available data. The western GoM has lower values of phase (60–80 days) whereas the eastern GoM has larger values of phase, with the largest value at the Florida coast (90–100 days). The phases at 60 and 100 days suggest Chl-a peaking around late January and late December, respectively. This suggests that the Chl-a peaking mostly occurs in wintertime in the main gulf. However, no significant phases are identified in the coastal regions, probably because the Chl-a concentration in the coastal regions is more dynamic. Fairly strong phase shift (−20 to 20 days) is revealed but only in small patches in the western and southeast gulf. Because primary production is relevant to multiple factors (nutrient, lights, temperature, etc.) and ocean currents and eddies, not just temperature, it is not surprising that no strong trends are observed.

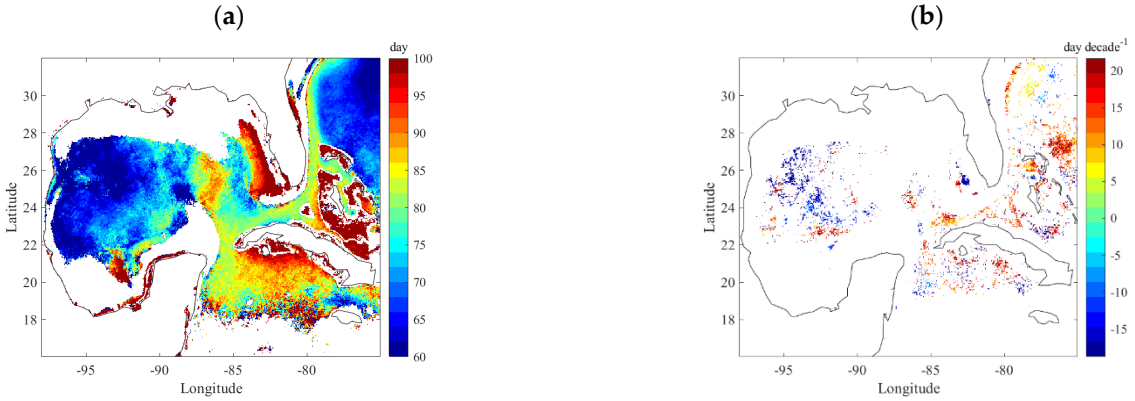

Figure 11. (**a**) Mean phase of Chl-a concentration during the 1997–2018 period; (**b**) rate of phase shift for Chl-a concentration during the 1997–2018 period, where the results with p-value > 0.1 are excluded in the plot.

3.3. Eddy-Related Energetic Features

Mesoscale eddies and variability in the GoM can have substantial impacts on heat and salt redistribution within the GOM [43,56] and climate extremes, e.g., hurricanes intensification [57–59]. It is still an open question whether and how the eddy activities are influenced in a warmer (Figures 4–6) and more windy GoM [7]. We examine if any trend can be detected for ocean eddies using the three eddy-related parameters defined in Section 2.3.3. Figure 12 shows the mean and maximal value of the three parameters that we used to quantify ocean eddies in the GoM. We took absolute value of vorticity and the Okubo–Weiss parameter so that we only quantify their magnitude and disregard the direction of rotation. All three parameters show a similar spatial pattern of the energetic ocean eddies. Most of these energetic features occur in the regions of loop current, loop current intrusion, and loop current eddies with water depths greater than 1000 m. This is consistent with the findings in Brokaw et al. [13] that the loop current region in the eastern GoM is an area of robust eddy generation for both cyclonic and anticyclonic eddies.

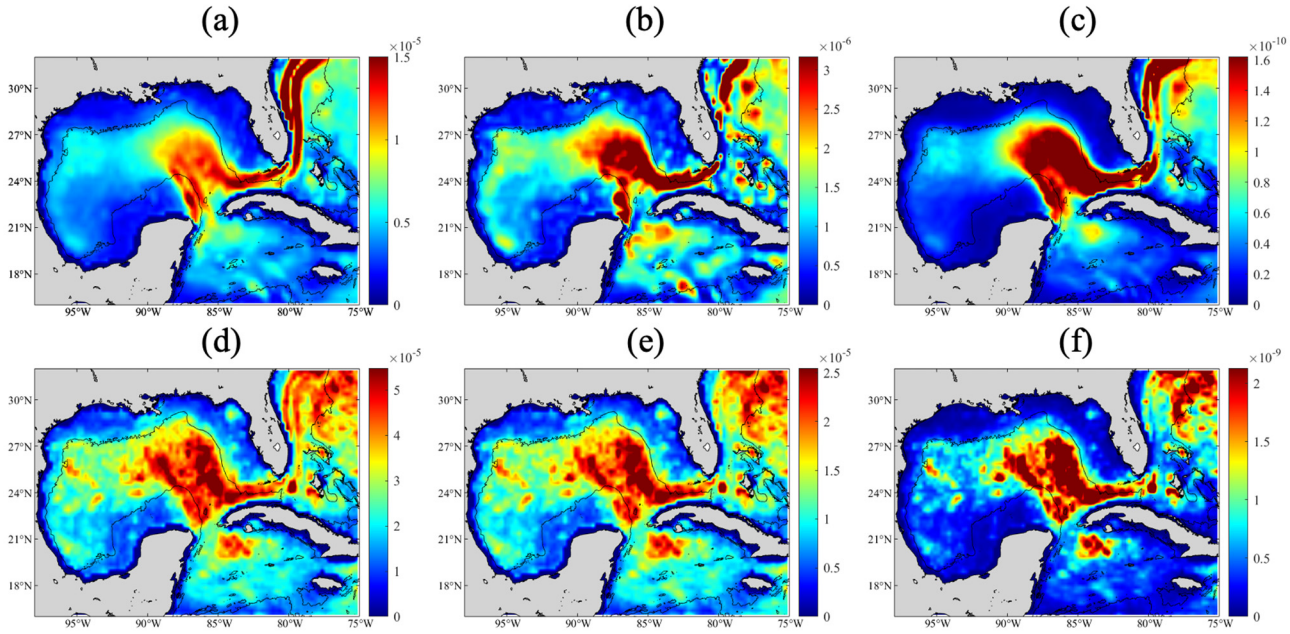

Figure 12. Spatial distribution of mean value for (**a**) absolute vorticity; (**b**) swirling strength; (**c**) absolute Okubo–Weiss parameter, and the maximal value for (**d**) absolute vorticity; (**e**) swirling strength; (**f**) absolute Okubo–Weiss parameter. The solid line shows a contour of 1000 m water depth. The units of vorticity and Okubo–Weiss parameter are s^{-1} and s^{-2}, respectively. Swirling strength is a dimensionless value.

The trends of all calculated eddy-related parameters are determined using linear regression, and the results are summarized in Table 1. Each column represents four eddy characteristics (i.e., area, strength, and intensity) calculated using each of the eddy-related parameters (absolute vorticity, swirling strength, and Okubo–Weiss parameter). Each row represents the same eddy characteristics calculated using three different parameters. Note that these values may represent different physical meanings. Mean, standard deviation, slope of linear regression, and the associated *p*-value are given in the Table.

Table 1. Trend of eddy-related parameters using linear regression for three eddy identification parameters during the 1993–2019 period. See Section 3.3 for a definition of each parameter. Note, the eddy-related features presented in this study are the strongest ones that exceed the percentile of 90% in the cumulative probability function of each parameter. The slope of the linear regression and its *p*-value of less than 0.05 are shaded in gray.

		Absolute Vorticity (s^{-1})	**Swirling Strength (−)**	**Absolute Okubo–Weiss Parameter (s^{-2})**
Area (km^2)	Mean value	1.3855×10^5	5.7026×10^4	2.7446×10^5
	Standard deviation	3.2647×10^4	1.5544×10^4	4.9428×10^4
	Slope of the regression (km^2/decade)	-3.7065×10^2	-9.0948×10^2	-2.9844×10^3
	p-value of regression	0.4052	1.7725×10^{-5}	9.4555×10^{-6}
Strength	Mean value	0.0038	8.1693×10^{-4}	1.9182×10^{-8}
	Standard deviation	9.9937×10^4	2.4407×10^{-4}	5.2887×10^{-9}
	Slope of the regression ([unit]/decade)	-3.8339×10^{-5}	-2.1015×10^{-5}	-6.1687×10^{-11}
	p-value of regression	0.0049	2.6258×10^{-10}	0.3924
Intensity	Mean value	2.3900×10^{-8}	1.3158×10^{-8}	1.4849×10^{-13}
	Standard deviation	1.0894×10^{-9}	6.5858×10^{-10}	1.0234×10^{-14}
	Slope of the regression ([unit]/decade)	-1.0741×10^{-10}	-8.6675×10^{-11}	4.6351×10^{-16}
	p-value of regression	4.5467×10^{-13}	3.9722×10^{-22}	8.9413×10^{-4}

Figure 13 shows an example of total strength defined using absolute vorticity, swirling strength, and absolute Okubo–Weiss parameter (see Table 1 for parameters of regression line). Here, we report the strongest eddy-related features (exceeding 90% percentile in the cumulative probability density function) as the representative of the most energetic ocean dynamics.

The regressions show that the total energetic areas in the GoM defined using swirling strength and Okubo–Weiss parameter show a decreasing trend, i.e., about 900 and 3000 km^2/decade decreasing rate, respectively. The per decade decreasing trend is about 1.6% and 1.1% of their mean values. The total strength also shows a slight decreasing trend based on absolute vorticity and swirling strength. Comparing with the mean value, the decreasing trend is about 1.0% and 2.6% for absolute vorticity and swirling strength, respectively. The intensity shows a decreasing trend in absolute vorticity (−0.4% per decade) and swirling strength (−0.6% per decade) but an increasing trend for the Okubo–Weiss parameter (+0.3% per decade). In general, these analyses show a statistically significant but small change in the most energetic eddy dynamics under a warming environment in the GoM.

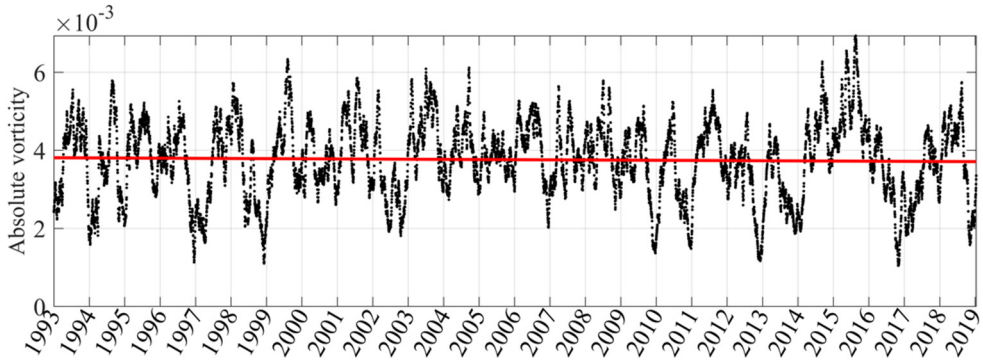

Figure 13. *Cont.*

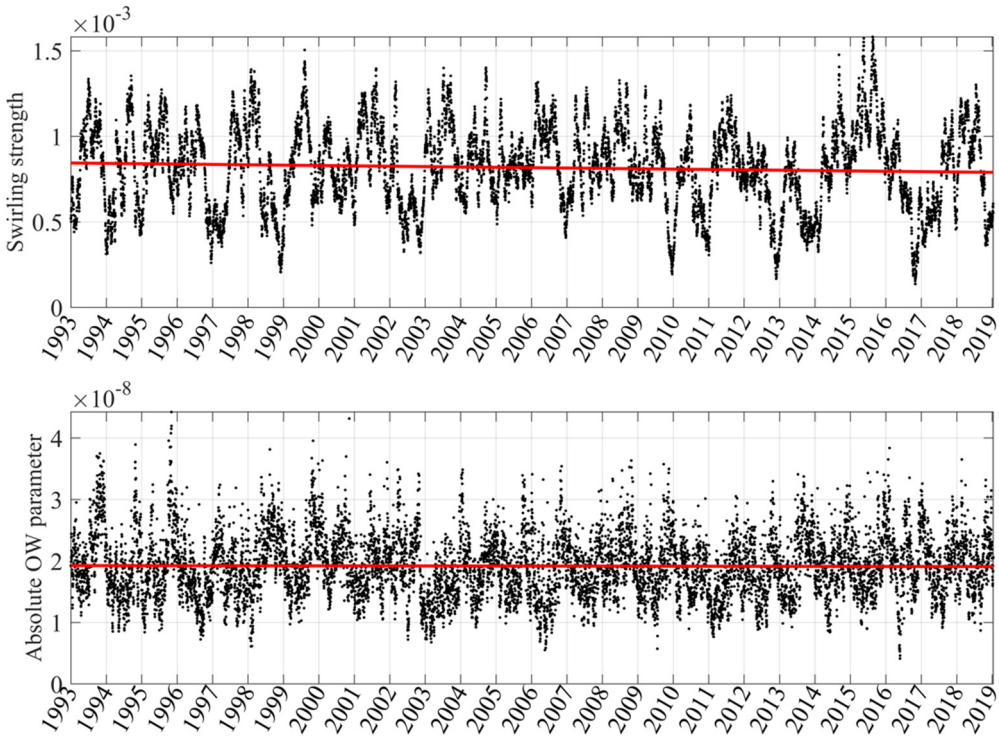

Figure 13. Trend of eddy parameters in the Gulf of Mexico using linear regression (red solid lines). The values are the summation of total strength that exceeds 90% percentile in the cumulative probability density function (i.e., the strongest eddies). Absolute values of vorticity and Okubo–Weiss parameter are taken. The units of vorticity and Okubo–Weiss parameter are s^{-1} and s^{-2}, respectively. Swirling strength is a dimensionless parameter. The regression results are summarized in Table 1.

4. Conclusions

Data for 38 years of SST (1982–2019), 22 years of Chl-a concentration (1997–2018), and 27 years of SSH (1993–2019) in the Gulf of Mexico are analyzed to investigate the trend of ocean dynamics in this economically important region for the United States, Mexico, and Cuba.

Linear regression is utilized to determine the trends, with supports of monthly down-sampling, phenological analysis, and per-grid scale analysis for spatial distributions. Our analysis finds that warming occurs everywhere at the surface of the GoM in all months except some coastal regions during wintertime. The strongest warming trends occur in April and October. Warmer seasons tend to have a larger warming trend than the cooler seasons. We found 1–4 days of phase shift in the northern coast of GoM, indicating that the annual cycle is shifting earlier in this region.

The data show high Chl-a concentration in the northern GoM coast with an increasing trend around the Mississippi River Delta. A clear phenological cycle is found in gulf-wide Chl-a and its rate of change. Mean Chl-a is relatively high in wintertime and remains relatively low from late February to early June and August. A secondary peak of Chl-a occurs during late June and early July, likely due to offshore dispersal of the Mississippi River and other coastal waters. The trend of Chl-a change seems to have some correlation with the Chl-a concentration, indicating potentially stronger variations. The monthly trend of Chl-a shows strong spatial variations. In general, increasing trends occur close to the Mississippi River Delta region and the Texas–Louisiana–Alabama coast. However, quite strong decreasing trends are present in the west of the Mississippi River Delta in February and March. Decreasing trends are often found at the Florida coast and the southwest gulf in the coastal region of Mexico. Phenological analysis indicates strong phase shift (−20 to 20 days) in small patches of the GoM.

Three eddy-indicating parameters are used to examine the trend of the strongest eddy dynamics (>90 percentile) in the GoM. Most of the eddy-relevant energetic features are in the regions of loop current, loop current intrusion, and loop current eddies with water depths greater than 1000 m. The data show a small but statistically significant trend of change in the areas, strength, and intensity. This result suggests that the warming GoM may experience some slow changes in dynamics of ocean eddies.

Author Contributions: Conceptualization, B.W. and Z.W.; methodology, G.L. and B.W.; formal analysis, G.L.; investigation, G.L.; resources, B.W.; data curation, G.L.; writing—original draft preparation, G.L., B.W. and Z.W.; writing—review and editing, B.W. and Z.W.; visualization, G.L.; supervision, B.W.; project administration, B.W.; funding acquisition, B.W. and Z.W. All authors have read and agreed to the published version of the manuscript.

Funding: This research is partially supported by a grant from the Microsoft AI for Earth. The corresponding author is grateful for the support by the National Academy of Sciences Gulf Research Program's Early Career Research Fellowship. This research is also partially supported by the NOAA grant 363541-191001-021000 (Northern Gulf Institute) at Mississippi State University.

Data Availability Statement: The data used in this study are available through various publicly accessible databases.

Conflicts of Interest: The authors declare no conflict of interest.

References

1. McCarthy, G.D.; Haigh, I.D.; Hirschi, J.J.-M.; Grist, J.P.; Smeed, D.A. Ocean impact on decadal Atlantic climate variability revealed by sea-level observations. *Nature* **2015**, *521*, 508–510. [CrossRef]
2. Spies, R.B.; Senner, S.; Robbins, C.S. An overview of the northern Gulf of Mexico ecosystem. *Gulf Mex. Sci.* **2016**, *33*, 9. [CrossRef]
3. Saunders, M.A.; Lea, A.S. Large contribution of sea surface warming to recent increase in Atlantic hurricane activity. *Nature* **2008**, *451*, 557–560. [CrossRef]
4. Dunstan, P.K.; Foster, S.D.; King, E.; Risbey, J.; O'Kane, T.J.; Monselesan, D.; Hobday, A.J.; Hartog, J.R.; Thompson, P.A. Global patterns of change and variation in sea surface temperature and chlorophyll a. *Sci. Rep.* **2018**, *8*, 14624. [CrossRef]
5. Muhling, B.A.; Lee, S.-K.; Lamkin, J.T.; Liu, Y. Predicting the effects of climate change on bluefin tuna (Thunnus thynnus) spawning habitat in the Gulf of Mexico. *ICES J. Mar. Sci.* **2011**, *68*, 1051–1062. [CrossRef]
6. Glenn, E.; Comarazamy, D.; González, J.E.; Smith, T. Detection of recent regional sea surface temperature warming in the Caribbean and surrounding region. *Geophys. Res. Lett.* **2015**, *42*, 6785–6792. [CrossRef]
7. Muller-Karger, F.E.; Smith, J.P.; Werner, S.; Chen, R.; Roffer, M.; Liu, Y.; Muhling, B.; Lindo-Atichati, D.; Lamkin, J.; Cerdeira-Estrada, S.; et al. Natural variability of surface oceanographic conditions in the offshore Gulf of Mexico. *Prog. Oceanogr.* **2015**, *134*, 54–76. [CrossRef]
8. Müller-Karger, F.E.; Walsh, J.J.; Evans, R.H.; Meyers, M.B. On the seasonal phytoplankton concentration and sea surface temperature cycles of the Gulf of Mexico as determined by satellites. *J. Geophys. Res. Ocean.* **1991**, *96*, 12645–12665. [CrossRef]
9. Behrenfeld, M.J.; O'Malley, R.T.; Boss, E.S.; Westberry, T.K.; Graff, J.R.; Halsey, K.H.; Milligan, A.J.; Siegel, D.A.; Brown, M.B. Revaluating ocean warming impacts on global phytoplankton. *Nat. Clim. Chang.* **2016**, *6*, 323–330. [CrossRef]
10. Wang, Z.; Boyer, T.; Reagan, J.; Hogan, P. Upper Oceanic Warming in the Gulf of Mexico between 1950 and 2020. In Proceedings of the GoMCon, Baton Rouge, LA, USA, 25–28 April 2022.
11. Ochoa, J.; Ferreira-Bartrina, V.; Candela, J.; Sheinbaum, J.; López, M.; Pérez-Brunius, P.; Herzka, S.; Amon, R.M. Deep-Water Warming in the Gulf of Mexico from 2003 to 2019. *J. Phys. Oceanogr.* **2021**, *51*, 1021–1035. [CrossRef]
12. Nowlin Jr, W.; Hubertz, J.; Reid, R. A detached eddy in the Gulf of Mexico. *J. Mar. Res* **1968**, *26*, 185–186.
13. Brokaw, R.J.; Subrahmanyam, B.; Trott, C.B.; Chaigneau, A. Eddy surface characteristics and vertical structure in the Gulf of Mexico from satellite observations and model simulations. *J. Geophys. Res. Ocean.* **2020**, *125*, e2019JC015538. [CrossRef]
14. Sturges, W.; Leben, R. Frequency of ring separations from the loop current in the Gulf of Mexico: A revised estimate. *J. Phys. Oceanogr.* **2000**, *30*, 1814–1819. [CrossRef]
15. Leben, R.R. *Altimeter-Derived Loop Current Metrics*; Geophysical Monograph-American Geophysical Union: Washington, DC, USA, 2005.
16. Chang, Y.L.; Oey, L.Y. Why does the Loop Current tend to shed more eddies in summer and winter? *Geophys. Res. Lett.* **2012**, *39*, L05605. [CrossRef]
17. Fratantoni, P.S.; Lee, T.N.; Podesta, G.P.; Muller-Karger, F. The influence of Loop Current perturbations on the formation and evolution of Tortugas eddies in the southern Straits of Florida. *J. Geophys. Res. Ocean.* **1998**, *103*, 24759–24779. [CrossRef]
18. Cochrane, J. Separation of an anticyclone and subsequent developments in the Loop Current (1969). *Contrib. Phys. Oceanogr. Gulf Mex.* **1972**, *2*, 91–106.

19. Androulidakis, Y.; Kourafalou, V.; Le Hénaff, M. Influence of frontal cyclone evolution on the 2009 (Ekman) and 2010 (Franklin) Loop Current eddy detachment events. *Ocean Sci.* **2014**, *10*, 947–965. [CrossRef]
20. Leben, R. Tracking Loop Current eddies with satellite altimetry. *Adv. Space Res.* **1993**, *13*, 325–333. [CrossRef]
21. Liu, Y.; Weisberg, R.H.; Vignudelli, S.; Mitchum, G.T. Patterns of the loop current system and regions of sea surface height variability in the eastern Gulf of Mexico revealed by the self-organizing maps. *J. Geophys. Res. Ocean.* **2016**, *121*, 2347–2366. [CrossRef]
22. Lewis, J.K.; Kirwan, A.D.; Forristall, G.Z. Evolution of a warm-core ring in the Gulf of Mexico: Lagrangian observations. *J. Geophys. Res.* **1989**, *94*, 8163–8178. [CrossRef]
23. Hamilton, P.; Fargion, G.S.; Biggs, D.C. Loop Current eddy paths in the western Gulf of Mexico. *J. Phys. Oceanogr.* **1999**, *29*, 1180–1207. [CrossRef]
24. Rivas, D.; Badan, A.; Sheinbaum, J.; Ochoa, J.; Candela, J. Vertical velocity and vertical heat flux observed within loop current eddies in the central Gulf of Mexico. *J. Phys. Oceanogr.* **2008**, *38*, 2461–2481. [CrossRef]
25. Putrasahan, D.; Kamenkovich, I.; Le Hénaff, M.; Kirtman, B. Importance of ocean mesoscale variability for air-sea interactions in the Gulf of Mexico. *Geophys. Res. Lett.* **2017**, *44*, 6352–6362. [CrossRef]
26. Brokaw, R.J.; Subrahmanyam, B.; Morey, S.L. Loop current and eddy-driven salinity variability in the Gulf of Mexico. *Geophys. Res. Lett.* **2019**, *46*, 5978–5986. [CrossRef]
27. Damien, P.; Sheinbaum, J.; Pasqueron de Fommervault, O.; Jouanno, J.; Linacre, L.; Duteil, O. Do Loop Current eddies stimulate productivity in the Gulf of Mexico? *Biogeosciences* **2021**, *18*, 4281–4303. [CrossRef]
28. Cardona, Y.; Bracco, A. Predictability of mesoscale circulation throughout the water column in the Gulf of Mexico. *Deep Sea Res. Part II Top. Stud. Oceanogr.* **2016**, *129*, 332–349. [CrossRef]
29. Hamilton, P.; Lee, T.N. Eddies and jets over the slope of the northeast Gulf of Mexico. In *Geophysical Monograph Series*; American Geophysical Union: Washington, DC, USA, 2005; Volume 161, pp. 123–142.
30. Androulidakis, Y.; Kourafalou, V.; Le Hénaff, M.; Kang, H.; Sutton, T.; Chen, S.; Hu, C.; Ntaganou, N. Offshore spreading of Mississippi waters: Pathways and vertical structure under eddy influence. *J. Geophys. Res. Ocean.* **2019**, *124*, 5952–5978. [CrossRef]
31. Justić, D.; Kourafalou, V.; Mariotti, G.; He, S.; Weisberg, R.; Androulidakis, Y.; Barker, C.; Bracco, A.; Dzwonkowski, B.; Hu, C. Transport Processes in the Gulf of Mexico Along the River-Estuary-Shelf-Ocean Continuum: A Review of Research from the Gulf of Mexico Research Initiative. *Estuaries Coasts* **2021**, *45*, 621–657. [CrossRef]
32. Sathyendranath, S.; Brewin, B.; Mueller, D.; Doerffer, R.; Krasemann, H.; Mélin, F.; Brockmann, C.; Fomferra, N.; Peters, M.; Grant, M. Ocean colour climate change initiative—Approach and initial results. In Proceedings of the 2012 IEEE International Geoscience and Remote Sensing Symposium, Munich, Germany, 22–27 July 2012; pp. 2024–2027.
33. Lian, T. Uncertainty in detecting trend: A new criterion and its applications to global SST. *Clim. Dyn.* **2017**, *49*, 2881–2893. [CrossRef]
34. Kelly, K.A.; Beardsley, R.C.; Limeburner, R.; Brink, K.H.; Paduan, J.D.; Chereskin, T.K. Variability of the near-surface eddy kinetic energy in the California Current based on altimetric, drifter, and moored current data. *J. Geophys. Res. Ocean.* **1998**, *103*, 13067–13083. [CrossRef]
35. Duran, R.; Nordam, T.; Serra, M.; Barker, C.H. *Marine Hydrocarbon Spill Assessments*; Makarynskyy, O., Ed.; Elsevier: Amsterdam, The Netherlands, 2021.
36. Zhou, J.; Adrian, R.J.; Balachandar, S.; Kendall, T. Mechanisms for generating coherent packets of hairpin vortices in channel flow. *J. Fluid Mech.* **1999**, *387*, 353–396. [CrossRef]
37. Adrian, R.; Christensen, K.; Liu, Z.-C. Analysis and interpretation of instantaneous turbulent velocity fields. *Exp. Fluids* **2000**, *29*, 275–290. [CrossRef]
38. Vortmeyer-Kley, R.; Gräwe, U.; Feudel, U. Detecting and tracking eddies in oceanic flow fields: A Lagrangian descriptor based on the modulus of vorticity. *Nonlinear Process. Geophys.* **2016**, *23*, 159–173. [CrossRef]
39. Reyes, O.; Manta, G.; Carrillo, L. Marine heatwaves and marine cold-spells on the Yucatan Shelf-break upwelling region. *Cont. Shelf Res.* **2022**, *239*, 104707. [CrossRef]
40. Tavakol, A.; Rahmani, V.; Harrington Jr, J. Evaluation of hot temperature extremes and heat waves in the Mississippi River Basin. *Atmos. Res.* **2020**, *239*, 104907. [CrossRef]
41. Martinez-Austria, P.F.; Bandala, E.R.; Patiño-Gómez, C. Temperature and heat wave trends in northwest Mexico. *Phys. Chem. Earth Parts A/B/C* **2016**, *91*, 20–26. [CrossRef]
42. Gunter, G. Mass mortality and dinoflagellate blooms in the Gulf of Mexico. *Science* **1951**, *113*, 250–251. [CrossRef]
43. Chang, Y.; Oey, L. Eddy and wind-forced heat transports in the Gulf of Mexico. *J. Phys. Oceanogr.* **2010**, *40*, 2728–2742. [CrossRef]
44. Leipper, D.F. A sequence of current patterns in the Gulf of Mexico. *J. Geophys. Res.* **1970**, *75*, 637–657. [CrossRef]
45. Sturges, W.; Evans, J.C. On the variability of the Loop Current in the Gulf of Mexico. *J. Mar. Res.* **1983**, *41*, 639–653. [CrossRef]
46. Behringer, D.W.; Molinari, R.L.; Festa, J.F. The variability of anticyclonic current patterns in the Gulf of Mexico. *J. Geophys. Res.* **1977**, *82*, 5469–5476. [CrossRef]
47. Liu, Y.; Weisberg, R.H.; Hu, C.; Kovach, C.; Riethmüller, R. *Evolution of the Loop Current System during the Deepwater Horizon Oil Spill Event as Observed with Drifters and Satellites*; American Geophysical Union: Washington, DC, USA, 2011; Volume 195, pp. 91–101. [CrossRef]

48. Liu, Y.; Weisberg, R.H.; Mooers, C.N.K. Performance evaluation of the self-organizing map for feature extraction. *J. Geophys. Res.* **2006**, *111*, C05018. [CrossRef]
49. Nickerson, A.K.; Weisberg, R.H.; Liu, Y. On the Evolution of the Gulf of Mexico Loop Current Through Its Penetrative, Ring Shedding and Retracted States. *Adv. Space Res.* **2022**, *69*, 4058–4077. [CrossRef]
50. Yang, Y.; Weisberg, R.H.; Liu, Y.; San Liang, X. Instabilities and multiscale interactions underlying the loop current eddy shedding in the Gulf of Mexico. *J. Phys. Oceanogr.* **2020**, *50*, 1289–1317. [CrossRef]
51. Stackpoole, S.; Sabo, R.; Falcone, J.; Sprague, L. Long-Term Mississippi River Trends Expose Shifts in the River Load Response to Watershed Nutrient Balances between 1975 and 2017. *Water Resour. Res.* **2021**, *57*, e2021WR030318. [CrossRef]
52. González, N.M.; Müller-Karger, F.E.; Estrada, S.C.; Pérez de los Reyes, R.; del Río, I.V.; Pérez, P.C.; Arenal, I.M. Near-surface phytoplankton distribution in the western Intra-Americas Sea: The influence of El Niño and weather events. *J. Geophys. Res. Ocean.* **2000**, *105*, 14029–14043. [CrossRef]
53. Pasqueron de Fommervault, O.; Perez-Brunius, P.; Damien, P.; Camacho-Ibar, V.F.; Sheinbaum, J. Temporal variability of chlorophyll distribution in the Gulf of Mexico: Bio-optical data from profiling floats. *Biogeosciences* **2017**, *14*, 5647–5662. [CrossRef]
54. Gilbes, F.; Tomas, C.; Walsh, J.J.; Müller-Karger, F.E. An episodic chlorophyll plume on the West Florida Shelf. *Cont. Shelf Res.* **1996**, *16*, 1201–1224. [CrossRef]
55. Martínez-López, B.; Zavala-Hidalgo, J. Seasonal and interannual variability of cross-shelf transports of chlorophyll in the Gulf of Mexico. *J. Mar. Syst.* **2009**, *77*, 1–20. [CrossRef]
56. Meza-Padilla, R.; Enriquez, C.; Liu, Y.; Appendini, C.M. Ocean Circulation in the Western Gulf of Mexico Using Self-Organizing Maps. *J. Geophys. Res. Ocean.* **2019**, *124*, 4152–4167. [CrossRef]
57. Shay, L.K.; Goni, G.J.; Black, P.G. Effects of a Warm Oceanic Feature on Hurricane Opal. *Mon. Weather Rev.* **2000**, *128*, 1366–1383. [CrossRef]
58. Jacob, S.D.; Shay, L.K. The Role of Oceanic Mesoscale Features on the Tropical Cyclone–Induced Mixed Layer Response: A Case Study. *J. Phys. Oceanogr.* **2003**, *33*, 649–676. [CrossRef]
59. Jaimes, B.; Shay, L.K. Near-Inertial Wave Wake of Hurricanes Katrina and Rita over Mesoscale Oceanic Eddies. *J. Phys. Oceanogr.* **2010**, *40*, 1320–1337. [CrossRef]